minerals

MDPI

Article

Microscopic Pore Structure Characteristics and Fluid Mobility in Tight Reservoirs: A Case Study of the Chang 7 Member in the Western Xin'anbian Area of the Ordos Basin, China

Qinlian Wei [1,2,*], Huifang Zhang [1,2], Yonglin Han [3], Wenjie Guo [4] and Ling Xiao [1,2,*]

1 School of Earth Science and Engineering, Xi'an Shiyou University, Xi'an 710065, China
2 Shaanxi Key Laboratory of Petroleum Accumulation Geology, Xi'an Shiyou University, Xi'an 710065, China
3 Department of Development, PetroChina Chaygiy Oillfield Company, Xi'an 710018, China
4 No. 2 Oil Production Plant, PetroChina Changqing Oilfield Company, Qingyang 735100, China
* Correspondence: wql@xsyu.edu.cn (Q.W.); xl@xsyu.edu.cn (L.X.)

Abstract: This research addresses the limited understanding of movable fluid occurrence characteristics in the Chang 7 reservoir by employing mercury injection capillary pressure, constant-rate mercury injections, and nuclear magnetic resonance methods. This study investigates the microscopic pore structure characteristics and movable fluids in the tight reservoir of the western Xin'an region, located in the Ordos Basin. The finding reveals that as permeability decreases, the distribution of the throat radius becomes more concentrated in the low-value area, resulting in a narrow distribution range with high curve peaks. Conversely, with an increasing permeability, the distribution range expands towards the high-value area while the curve peak decreases. This research underscores the significance of the throat radius, especially the main flow throat radius, in constraining the permeability of rock samples. Furthermore, this study highlights a stronger correlation between permeability and movable fluid saturation than porosity. This finding emphasizes the importance of considering movable fluid saturation when assessing reservoir characteristics. Notably, the throat radius plays a crucial role in influencing the occurrence characteristics of movable fluids, with a smaller throat radii posing hindrances to fluid flow in the reservoir. Additionally, the presence of clay minerals in the reservoir leads to pore segmentation and increased fluid flow resistance, ultimately reducing the saturation of movable fluids. I must be understood that these factors are essential for developing and producing reservoirs with similar characteristics. In conclusion, the insights gained from this study hold considerable theoretical value and provide essential references for developing and producing reservoirs with tight characteristics, particularly in the western Xin'an region of the Ordos Basin.

Keywords: tight reservoir; micropore structure; movable fluid; mainstream throat radius; permeability; porosity; ordos basin

check for updates

Citation: Wei, Q.; Zhang, H.; Han, Y.; Guo, W.; Xiao, L. Microscopic Pore Structure Characteristics and Fluid Mobility in Tight Reservoirs: A Case Study of the Chang 7 Member in the Western Xin'anbian Area of the Ordos Basin, China. *Minerals* **2023**, *13*, 1063. https://doi.org/10.3390/min13081063

Academic Editor: Stanisław Mazur

Received: 27 June 2023
Revised: 3 August 2023
Accepted: 8 August 2023
Published: 11 August 2023

1. Introduction

Recently, there has been a growing emphasis on developing and utilizing unconventional oil and gas resources due to the surging global energy demand and the diminishing traditional reservoir reserves [1–5]. Tight reservoirs, defined as those with a porosity below 10% and permeability of the overburden less than 0.1 mD, have garnered considerable attention among unconventional hydrocarbon reservoirs in research circles [1,2,4].

The pore structure of reservoirs reflects the shape, size, geometry, spatial distribution characteristics, and connectivity of pores and throats. Various techniques are available for evaluating pore structures, including thin sections, scanning electron microscopy (SEM), mercury injection capillary pressure (MICP), and nuclear magnetic resonance (NMR) [1,2]. Combining these methods can provide a complementary approach to more accurately and precisely characterize the pore structures of tight/shale oil formations that exhibit

strong heterogeneity. At present, the research on the micropore structure of reservoirs lacks comprehensive investigations regarding the fluidity saturation of reservoirs [6–9]. Fluid mobility reflects the reservoir quality and impacts its development potential [10,11]. Several experimental techniques have been employed to investigate tight oil mobility, including environmental scanning electron microscopy combined with quantitative grain fluorescence (QGF) [12], nuclear magnetic resonance (NMR) [13,14], and core displacement through physical simulation [15].

The existing studies on the Late Triassic tight reservoirs have primarily concentrated on parameters like porosity, permeability, and micropore structure in the Ordos Basin [16,17]. However, when assessing reservoir effectiveness, researchers have frequently treated the evaluation of reservoir pore structure and movable fluids as separate entities, leading to a lack of transparent linkage between the two and an absence of research on the contribution of different reservoir spaces to permeability and the corresponding movable fluids.

This study aims to investigate the relationship between mobile fluids and pore structure by analyzing the factors influencing fluid saturation, using the Chang 7 reservoir of the western Xin'anbian area, Ordos Basin, as a specific case study. This investigation will be carried out through the utilization of constant-rate mercury injection (CRMI), mercury injection capillary pressure (MICP), and nuclear magnetic resonance techniques (NMR), forming a comprehensive approach to the analysis. This study holds immense significance in elucidating the mechanism of fluid migration and reservoir efficiency, offering valuable insights for optimizing development processes and technical approaches to achieve the efficient and sustainable exploitation of unconventional oil and gas.

2. Geology Setting

The Ordos Basin, a vast sedimentary craton basin located on the North China plate, is China's second-largest inland sedimentary basin. It holds considerable oil and gas reserves, making it a prominent hydrocarbon-bearing region [18,19]. During the middle and late Triassic period, known as the Yanchang Formation sedimentary period, the basin underwent a transformation into a vast inland craton depression lake basin. Over this period, significant continental clastic rock sedimentary formations were deposited, with a combined thickness exceeding 1000 m. The Yanchang Formation is typically classified into ten stratigraphic units labeled from Chang 10 to Chang 1 sequentially from bottom to top (Figure 1b).

The Chang 7 sedimentary period marks a remarkable event in the Mesozoic basin, characterized by extensive lake flooding. Semi-deep lakes with depths ranging from 5 to 20 m and deep lake areas reaching depths of 20 to 150 m expanded, primarily distributed in the southwestern region of the basin [20]. During this period, these lakes supported a thriving ecosystem of algae and planktonic organisms. Additionally, frequent thermal fluid activities enriched the basin, contributing to the formation of organic shale. As a result, a significant thickness of organic-rich source rock series exceeding 100 m developed within the basin (Figure 1a).

The western part of the Xin'anbian area is situated on the northern Shaanxi slope in the central-western segment of the basin, featuring a gently westward dipping monocline in its structural geology (Figure 1a). Several factors, including the northeastern, northwestern, and southwestern source areas, primarily influenced the Chang 7 sedimentary period in the study area. Among these factors, the northeastern and northwestern source areas played a particularly significant role in shaping the characteristics of the study area. During the Chang 7 sedimentary period, the dominant sedimentary facies comprised delta front to deep lake deposits.

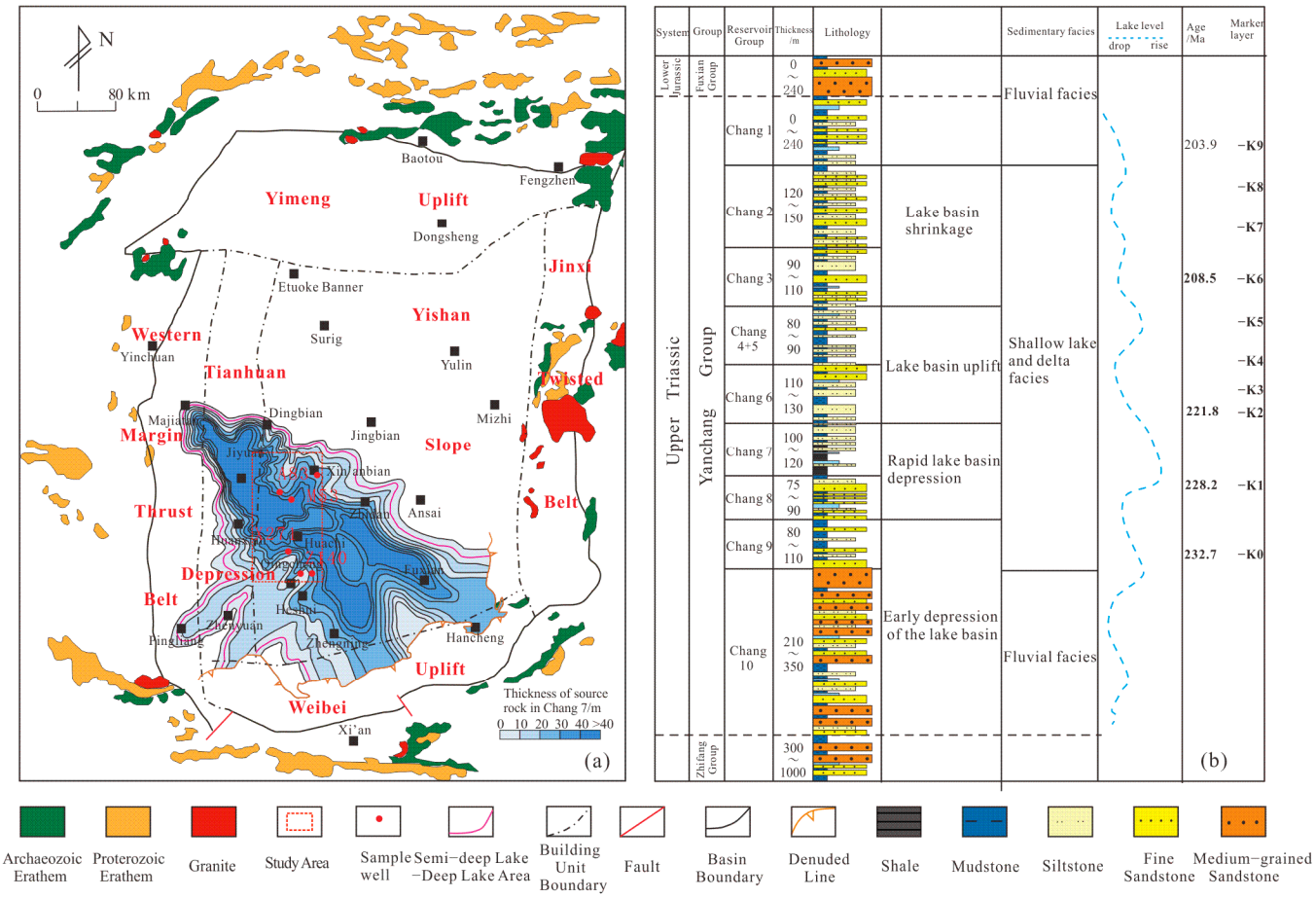

Figure 1. Location of the research area and target horizon. (**a**) is the location map of the research area; (**b**) is stratigraphic column of Yangchang group.

3. Materials and Methods

The study utilized 189 thin sections and carried out three scanning electron microscopy (SEM) analyses to determine the reservoir's mineral composition and pore characteristics. Furthermore, the reservoir's quality was evaluated based on the findings from 1200 rock physical property tests. The thin sections, SEM analysis, and petrophysical property assessments were carried out by the Shaanxi Key Laboratory of Oil and Gas at Xi'an Shiyou University.

To determine the petrophysical properties of the rocks, a CMS-300, which employs helium and nitrogen as working media and has a pressure sensor accuracy of 0.1%, was utilized. Mercury injection capillary pressure (MICP) experiments were conducted using an Autopore IV-9520 manufactured by American Mike. The instrument effectively operated within a pressure range of 0 to 206.7 megapascal (MPa), enabling the measurement of a pore throat radius as small as approximately 3.6 nm.

The ASPE-730 constant-rate mercury injection (CRMI) experimental instrument was used to analyze pore structure characteristics, providing precise parameters, including the average throat radius.

Additionally, nuclear magnetic resonance (NMR) measurements were performed using a Magnet2000 instrument. The measurements were consistently conducted at a temperature of 20 °C. NMR, a non-invasive method, allowed the analysis of reservoir dynamics. The MICP, CRMI, and NMR experiments were carried out by the Langfang Branch of China Petroleum Exploration and Development Research Institute. This study will further employ these experimental methods to investigate the dynamics of mobile

fluids in tight reservoirs and explore the correlation of the pore structure characteristics with the behavior of mobile fluids in such reservoirs.

4. Results

4.1. Reservoir Petrology and Mineralogy Characteristics

The primary lithology of the Chang 7 reservoir sandstone in the western part of the Xin'anbian area is primarily composed of gray and grayish-black fine sandstones. The predominant rock types include arkose and lithic arkose, with smaller amounts of feldspathic litharenite and litharenite (Figure 2a). Based on the statistical analysis of thin sections, it can be observed that the average content of mineral and rock debris is distributed as follows: quartz accounts for 29.27%, feldspar for 31.94%, and lithics for 16.19% (Figure 2b).

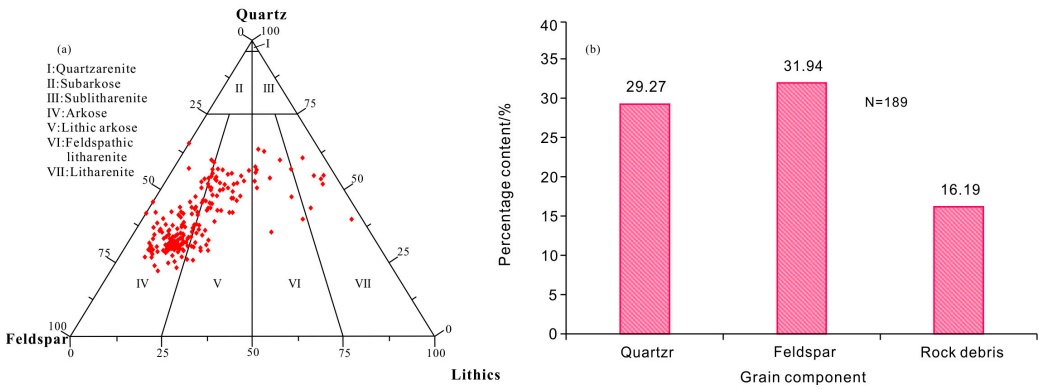

Figure 2. Rock type and particle composition characteristics. (**a**) Ternary diagram of Chang 7 sandstone composition in the west Xin'anbian, Ordos Basin; (**b**) characteristics of grain components.

In the study area, the total amount of interstitial materials, including both matrix and cement, in the Chang 7 reservoir is 23.1%. Among these materials, the highest content is illite, followed by ferrocalcite and chlorite interstitial material, with siderite content being the lowest (Figure 3). The figure shows three distinct areas in the content distribution details of clay minerals. The highest relative proportion of clay mineral content is found in less than 2%, accounting for 17.2%. The second area with a relatively high proportion lies in the range where the clay mineral content exceeds 14%, comprising 16.1% of the distribution. The third region displaying a higher distribution is the 4%–6% range, with a relative proportion of 15.2% (Figure 4).

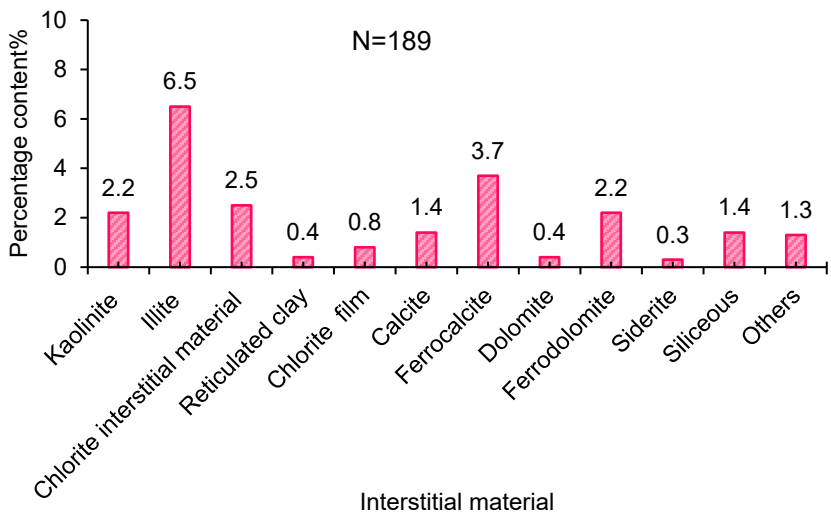

Figure 3. Contents and types of interstitial material.

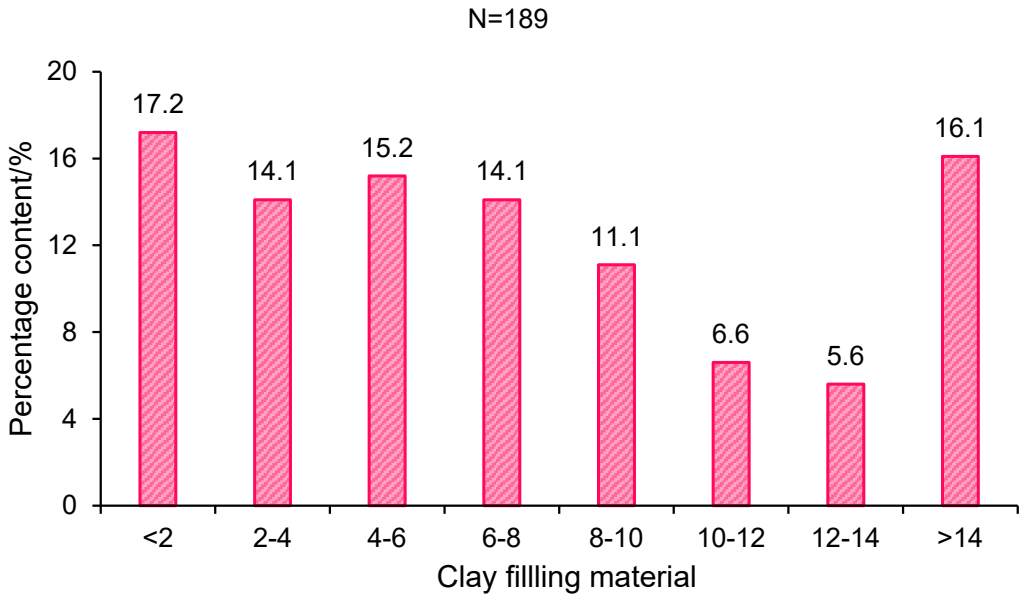

Figure 4. Total amount of clay-filling material.

Illite is a common clay mineral in the Chang 7 reservoir located in the study area, which is mainly formed in early diagenetic stage B (Figure 5), and part of Illite is formed in Mesogenetic diagenetic stage A2 [21]. Observations reveal that it mainly appears as flaky and filamentous aggregates, adhering either to particle surfaces in a filmy manner or extending along the surfaces and into the pores and pore throats, as observed through SEM analysis (Figure 6a).

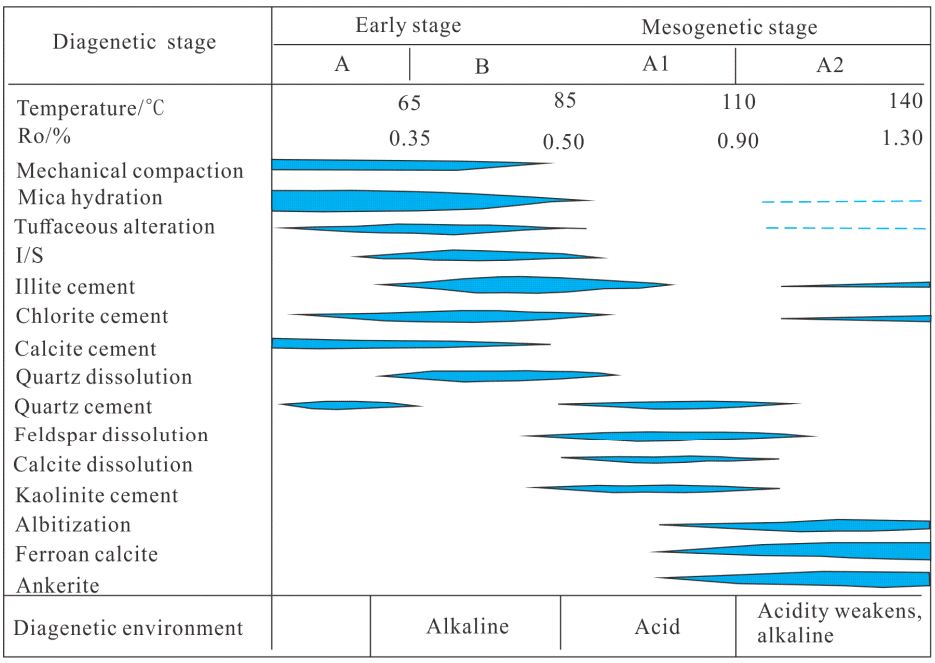

Figure 5. Diagenetic evolution sequence of Chang 7 reservoir.

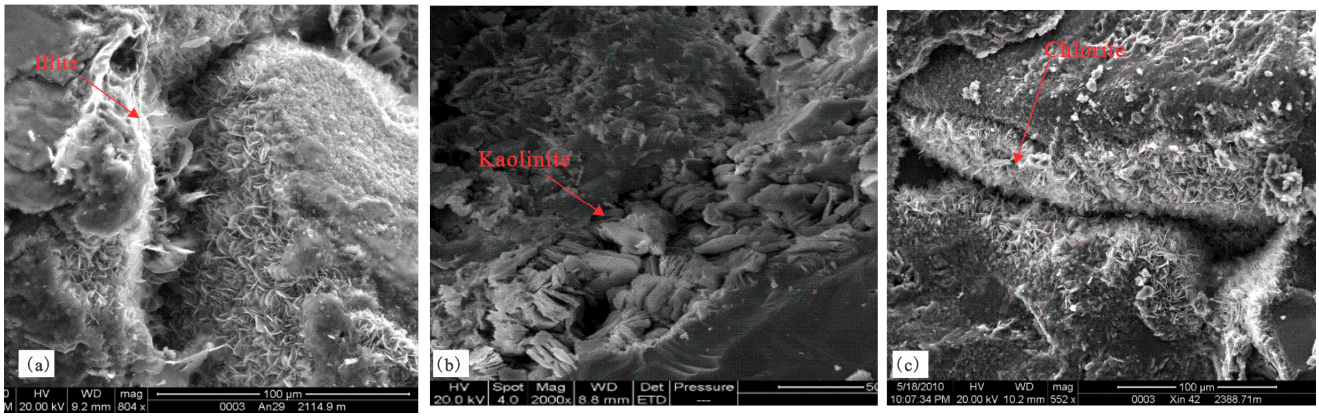

Figure 6. SEM characteristics of major clay cements (**a**) Filamentous illite filling intergranular pore throat, Well An 292,114.9 m, Chang 7; (**b**) pore-filling kaolinite, Well Geng 282, Chang 7, 2445.5 m; (**c**) chlorite group film, Well Xin 42, Chang 7, 2388.7 m).

Kaolinite is primarily present as pore-filling material in the Chang 7 reservoir. Most of the authigenic kaolinite fills the intergranular pores of the sandstone as dispersed particles. These particles often form complete pseudo-hexagonal euhedral crystals or aggregate into various forms, such as plate-shaped and worm-shaped structures (Figure 6b).

Chlorite represents another significant cement type in the sandstone of the Chang 7 Member. In the study area, chlorite minerals predominantly occur in leaf-like shapes and act as filmy pore linings (Figure 6c).

4.2. Reservoir Physical Characteristics

In the western region of Xin'anbian, the porosity distribution of the Chang 7 sandstone cores primarily ranges between 6% and 8%, with an average porosity of 7.0% (Figure 7a). Most permeability values are concentrated below 0.05 mD, followed by the 0.05 to 0.2 mD range (Figure 7b). A positive correlation exists between permeability and porosity, as the permeability value increases with a rise in porosity (Figure 7c).

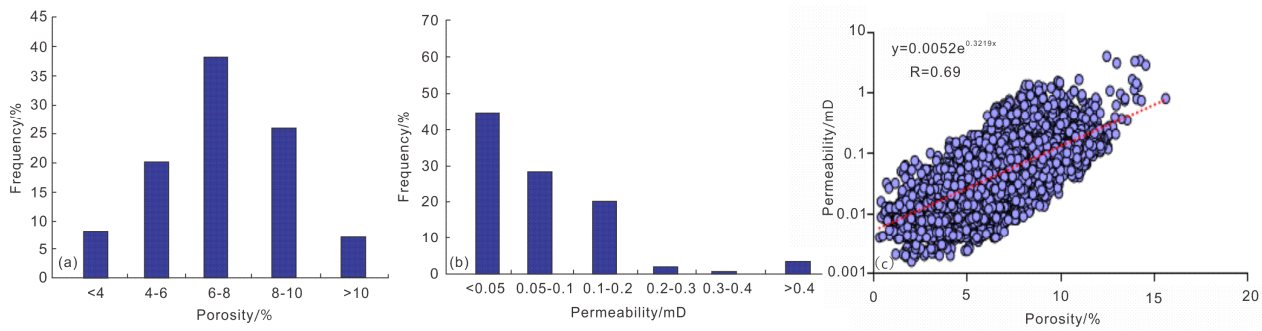

Figure 7. Physical property characteristics of the Chang 7 reservoir in the Western Xin'anbian. (**a**) Porosity distribution; (**b**) permeability distribution; (**c**) scatter plot of porosity and permeability).

4.3. Microscopic Pore Throat Structure Characteristics of Reservoirs

4.3.1. Investigation of Microscopic Pore Structure Characteristics Using CRMI

CRMI technology, which overcomes the limitations of conventional methods, enables precise throat measurement [22]. It is an advanced technique for studying the characteristics of pore structures, allowing separate measurements of parameters related to pores and throats. The findings from constant velocity mercury injection testing conducted on ten cores from the Chang 7 reservoir are presented in Table 1.

Table 1. Main parameter of CRMI on tight reservoir.

Well	Porosity/%	Permeability/mD	Maximum Throat Radius/μm	Everage Throat Radius/μm	Mainstream Throat Radius/μm
Y76	7.61	0.018	0.4	0.146	0.152
L17	7.72	0.020	0.4	0.261	0.288
B89	9.06	0.025	0.6	0.339	0.321
M53	8.17	0.027	0.5	0.269	0.291
Z180	7.27	0.029	0.5	0.289	0.315
X271	8.57	0.035	0.5	0.290	0.317
J46	9.14	0.052	0.6	0.306	0.321
N45	7.41	0.062	0.6	0.296	0.311
X270	9.05	0.078	0.7	0.397	0.465
J46-2	10.08	0.098	0.9	0.511	0.485

CRMI curves reveal significant variations in the distribution of throat radii among cores with different permeability levels (Figure 8). Specifically, cores with lower permeability display a more concentrated distribution of throat radii in the lower value range (Figure 8a,b), characterized by a narrow range and a pronounced peak curve. Conversely, as permeability increases, the distribution range expands towards higher values, albeit with a diminishing peak curve (Figure 8c). This observation suggests that the throat radius predominantly governs the permeability of rock samples.

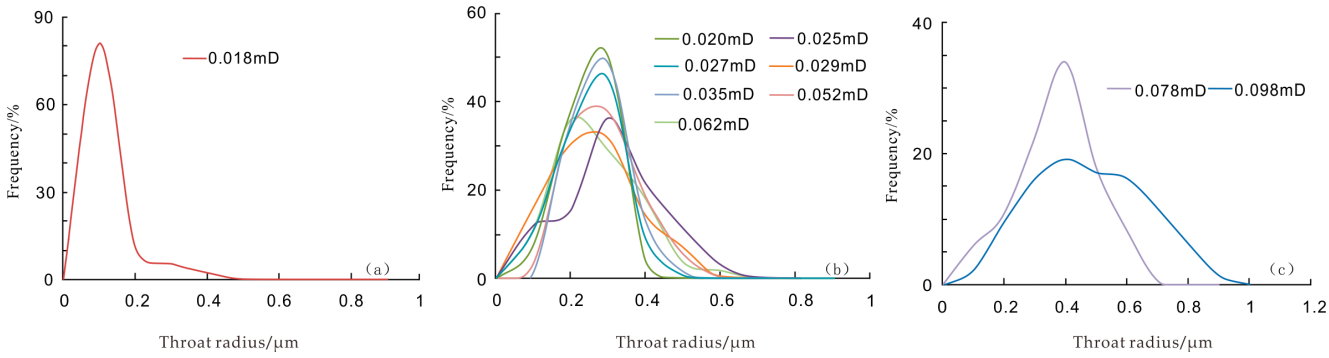

Figure 8. Distribution curve of core throat radius. (**a**) Permeability is in the range of very low, less than 0.02 mD; (**b**) permeability falls within a moderate range, greater than 0.02 mD but less than 0.07 mD; (**c**) permeability is relatively high, greater than 0.07 mD.

The mainstream throat radius of the core can be determined through the utilization of CRMI, which represents the weighted average of all throat radii, where the contribution to core permeability reaches 95% [23]. The magnitude of this value directly reflects the core's seepage capability. A smaller mainstream throat radius signifies more significant challenges in extraction. Figure 9 shows that's sandstone cores with a permeability below 0.02 mD exhibit a mainstream throat radius of approximately 0.1 μm. In the case of permeability ranging from 0.02 to 0.07 mD, the mainstream throat radius averages around 0.3 μm. For permeability exceeding 0.07 mD, the mainstream throat radius measures approximately 0.4 μm.

4.3.2. Investigation of Microscopic Pore Structure Characteristics Using MICP

MICP allows for the measurement of pore radii ranging from 1.8 nm to 500 μm, enabling the comprehensive visualization of pore throat spatial distribution in low-permeability samples [22]. This research conducted MICP on 12 cores obtained from the Chang 7 reservoir. The capillary pressure curves of cores with different permeability levels display a uniform shape with a relatively even middle portion, implying a focused distribution of pore throats, organized arrangement, and cohesive internal consistency within the cores (Figure 10). As

the permeability increases, the curve gradually shifts towards the left, while the maximum mercury saturation remains around 80% (Table 2).

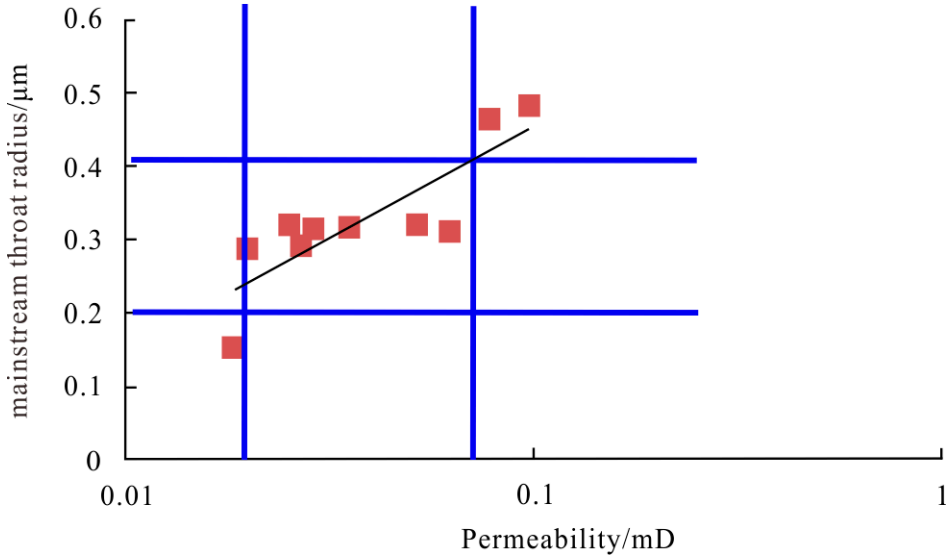

Figure 9. The relation between mainstream throat radius and permeability in the Chang 7 reservoir.

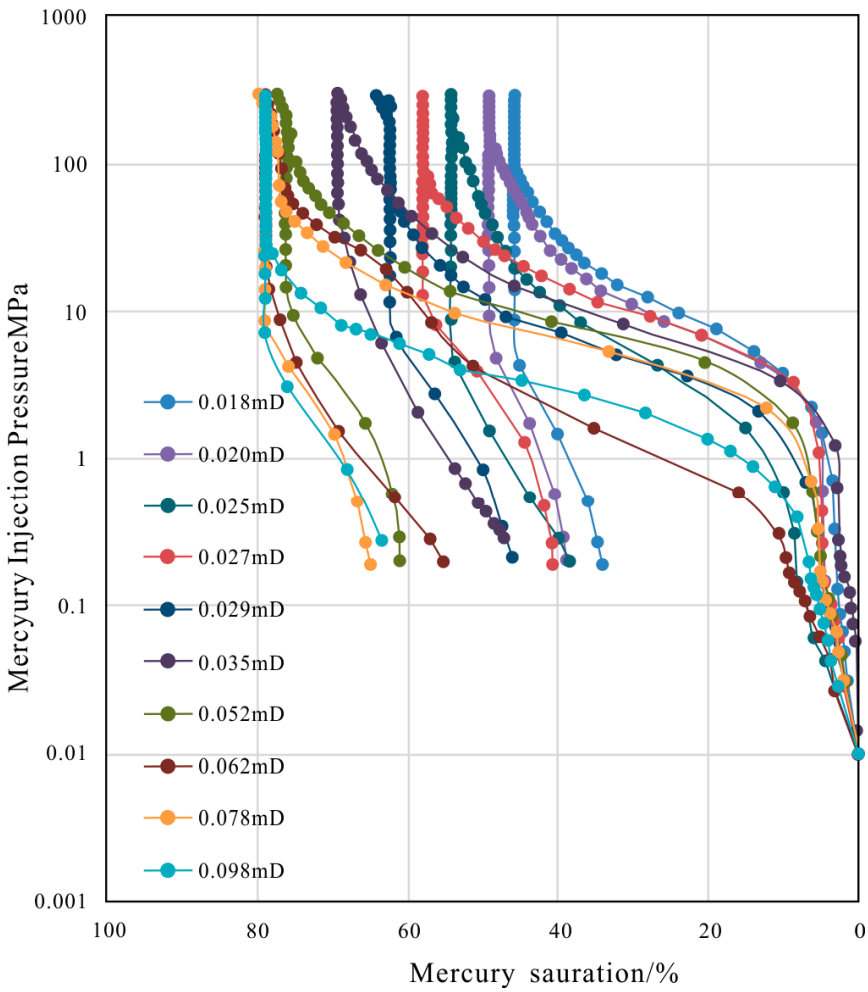

Figure 10. Typical capillary curve characteristics of the Chang 7 reservoir.

Table 2. The main result of MICP.

Well	Porosity/%	Permeability/mD	Average Pore Radius/μm	Sorting Coefficient	Maximum Mercury Saturation/%	Displacement Pressure/MPa	Median Saturation Pressure/MPa
Y76	7.61	0.018	0.11	5.15	45.92	0.72	***
Z140	7.41	0.020	0.06	4.08	49.23	1.76	***
B89	9.06	0.025	0.07	5.40	54.36	1.12	30.12
M53	8.17	0.027	0.38	5.83	58.01	0.20	3.83
Z180	7.27	0.029	0.09	3.80	64.45	0.72	8.97
X271	8.57	0.035	0.16	3.68	69.44	0.32	12.22
J46	9.14	0.052	0.26	4.66	77.57	0.31	4.10
N45	7.41	0.062	0.08	3.94	79.06	0.60	12.09
X270	9.05	0.078	0.06	3.53	79.67	1.25	20.14
J46-2	10.08	0.098	0.18	5.53	79.88	0.31	49.48

Note: "***" indicates missing data.

The relationship between the pressure of mercury saturation and the pore throat radius is obtained from the following Equation (1) [24]:

$$P_c = 2\alpha \cos \theta / r \tag{1}$$

where α indicates the interfacial tension, α = 480 mN/m, θ denotes the contact angle, $\theta = 140°$, r represents the pore throat radius in μm, and P_c represents the pressure of mercury saturation in MPa.

In this study, the Wall method was employed, with the incremental pore volume as the measurement metric, to establish the relationship between pore throat radius and permeability [6]. By converting the pressure, we obtained the distribution of pore throats and the corresponding distribution of permeability contribution for each core (Table 3).

The calculation of permeability contribution for an individual throat is performed as follows [25]:

$$\Delta K_i = \left[(2i-1)r_i^2\right] \Big/ \left[\sum_i^n (2i-1)r_i^2\right] \tag{2}$$

where ΔK_i represents the permeability contribution of pore throats in different radius, and r_i represents a pore throat radius in μm.

The proportions of various pore throat intervals and their corresponding permeability distributions can be calculated using Equation (2) (Table 3). The characteristics of various pore structures and their individual impacts on permeability distribution are illustrated in Figure 11.

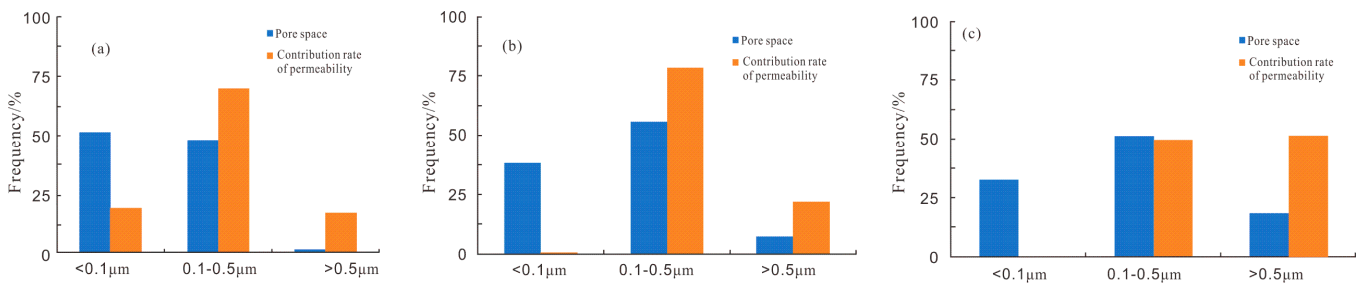

Figure 11. Distribution of reservoir pore space and permeability contribution. (**a**) Type III of pore structure, permeability < 0.1 mD; (**b**) type II of pore structure, permeability 0.1–0.2 mD; (**c**) type I of pore structure, permeability greater than 0.2 mD.

Figure 11a indicates that for permeabilities below 0.1 mD, the dominant flow space measures less than 0.1 μm (Figure 11a). In the case of permeabilities ranging from 0.1 to 0.2 mD (Figure 11b), the main storage and primary flow space are characterized by pores in the range of 0.1–0.5 μm. However, for permeabilities exceeding 0.2 mD (Figure 11c), the primary storage space comprises pores within the 0.1–0.5 μm range, while the primary flow space consists of pores larger than 0.1 μm.

Table 3. Distribution of pore throats and permeability contributions of different sandstone cores.

Type	Well	Porosity/%	Permeability/mD	Maximum Pore Radius/μm	Average Pore Radius/μm	Mainstream Throat Radius/μm	Pore Throat Ratio and Permeability Distribution in Different Pore Throat Intervals					
							<0.1 μm		0.1–0.5 μm		>0.5 μm	
							Pore Throat Ratio/%	Contribution Rate of Permeability/%	Pore Throat Ratio/%	Contribution Rate of Permeability/%	Pore Throat Ratio/%	Contribution Rate of Permeability/%
III	Y76	7.608	0.018	0.109	0.057	0.060	99.76	99.21	0.24	0.79		
	Z183	7.415	0.020	0.470	0.079	0.110	71.32	19.64	28.68	80.36		
II	B89	9.064	0.025	0.502	0.117	0.108	57.61	21.42	42.15	67.40	0.24	11.18
	M53	8.175	0.027	0.563	0.118	0.175	57.44	16.83	42.47	80.66	0.08	2.50
	Z183	7.265	0.029	0.300	0.159	0.172	26.27	1.65	73.73	98.34		
	X233	8.569	0.035	1.027	0.195	0.209	34.85	2.21	63.31	61.59	1.84	36.19
	A83	9.137	0.052	0.594	0.170	0.221	33.81	2.93	65.81	93.25	0.39	3.81
	N89	7.412	0.062	1.255	0.274	0.401	34.54	0.66	63.47	74.42	1.99	24.91
I	X233	9.046	0.078	0.866	0.161	0.421	46.65	4.71	52.29	74.40	1.05	20.89
	A83-2	10.080	0.098	1.020	0.277	0.468	41.67	0.81	51.93	66.99	6.40	32.20
	N89	10.53	0.147	1.240	0.285	0.486	37.76	0.44	55.43	78.06	6.81	21.50
	X233	10.26	0.250	1.480	0.297	0.504	31.70	0.34	50.44	48.95	17.86	50.71

4.4. Investigation of Mobile Fluids

NMR has emerged as the predominant method for acquiring pore throat data, owing to its exceptional capability to retrieve fluid and pore throat parameters rapidly and accurately within porous media [26]. In the NMR experiment, the remaining water saturation in the rock sample was determined under a centrifugal force of 417 psi, and the mobile fluid was completely extracted at 417 psi. As a result, the percentage of movable fluid can be calculated by subtracting the remaining water saturation from 100%. In this study, movable fluid testing and analysis were carried out on 20 cores obtained from the Chang 7 reservoir (Table 4), which indicated that the average of movable fluid is 31.96%. At permeability levels below 0.1 mD, the proportion of movable fluid content is determined to be 23.95%. For permeabilities ranging from 0.1 to 0.2 mD, the movable fluid content reaches 40.65%. Furthermore, permeabilities exceeding 0.2 mD exhibit a movable fluid content of 49.07%.

Table 4. Results of NMR for mobile fluid.

Well	Depth/m	Porosity/%	Permeability/mD	Percentage of Movable Fluid/%
Y76	2126.00	7.61	0.018	11.23
Z140	1814.20	7.42	0.020	14.61
B89	2475.00	9.06	0.025	12.04
M53	2221.00	8.18	0.027	18.91
Z180	1890.00	7.27	0.029	35.78
X271	2035.00	8.57	0.035	31.94
A83	2277.28	9.13	0.052	26.72
N45	1692.00	7.41	0.062	25.46
X270	2047.60	9.05	0.078	17.77
J46-2	2275.02	10.08	0.100	38.18
X70	1635.10	10.53	0.150	41.27
X270-1	2042.70	10.26	0.250	51.25
X270-2	2043.47	9.43	0.15	51.25
N70	1635.10	10.53	0.15	41.27
L399	2117.14	7.75	0.02	17.60
YC1	1984.66	8.99	0.09	18.27
X270-3	2044.90	11.83	0.10	29.87
J46-2	2275.02	10.08	0.10	38.18
H283	2302.70	11.14	0.20	47.00
X233	1932.50	9.51	0.03	25.06

5. Discussion

5.1. Distribution of Mobile Fluid in the Reservoir

NMR centrifugation analysis of mobile fluids plays a vital role as an experimental method for assessing reservoir matrices' storage capacity and potential, allowing us to determine the percentage of movable and flowing pores present in the reservoir [25].

This study provides movable fluids controlled by each sandstone core in different throat radius intervals, studies the reservoir matrix storage capacity and the size of movable pore space within specific throat intervals, and provides a basis for evaluating reservoir classification and research on availability. The movable fluid content controlled by different aperture intervals calculated based on different centrifugal forces is shown in Figure 12.

Based on the observations from Figures 4 and 7, it is evident that the percentage of movable fluids larger than 1.0 μm is relatively insignificant, with the vast majority of movable fluids predominantly governed by nanoscale (less than 0.1 μm) and submicron (0.1–1.0 μm) throats. As the permeability increases, the number of movable fluids controlled by nanoscale and submicron throats also increases, indicating a higher development potential.

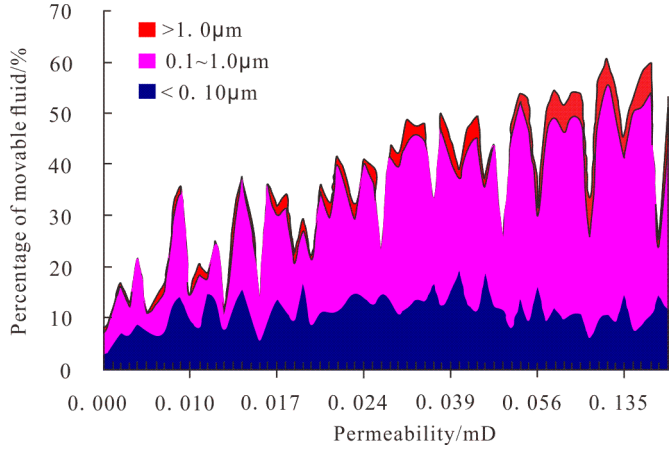

Figure 12. Distribution of mobile fluid in the reservoir.

5.2. Impact of Reservoir Physical Properties on Movable Fluid Saturation

Several researchers suggest that reservoir physical properties are vital in influencing movable fluid saturation [27,28]. In this investigation, a comparative analysis was performed to determine the relative impact of porosity and permeability on their correlation with movable fluid saturation. NMR revealed a positive correlation of movable fluid saturation with porosity, followed by an exponential function (Figure 13a). Furthermore, a similar exponential association was observed between the saturation of movable fluids and permeability, accentuating a substantial augmentation in saturation levels with higher permeability values (Figure 13b). Among these factors, permeability was found to have a more pronounced impact. Research has indicated that the correlation of permeability with movable fluid saturation surpasses that of porosity. The observed discrepancy arises because movable fluids are primarily influenced by pore connectivity, whereas porosity only accounts for the presence of effective pores and fails to capture the inter-pore connectivity. Consequently, the correlation between movable fluid saturation with porosity is weak.

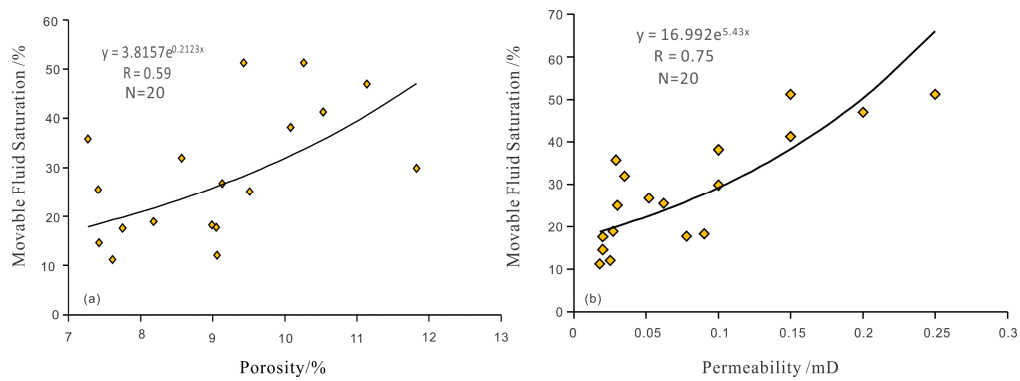

Figure 13. Correlation between mobile fluid content, porosity, and permeability in tight reservoirs. (**a**) The Correlation Between Porosity and mobile fluid saturation; (**b**) The Correlation Between Permeability and mobile fluid saturation.

Indeed, there is a poor correlation between the physical properties of tight reservoirs and the saturation of movable fluids. Consequently, even where porosity and permeability values are relatively close, the saturation of movable fluids in the reservoir may exhibit significant differences due to variations in pore structure.

5.3. Impact of Pore Structure on Movable Fluid Saturation

Analyzing reservoir pore structure entails studying pore and throat types, content, size, distribution, and connectivity [28,29]. These factors are essential in comprehending the reservoir's microscopic characteristics and seepage behavior.

It can be seen that the parameters of the movable fluid are positively correlated with the average porosity (Figure 14a) and mainstream throat radius (Figure 14b). However, there is no significant positive correlation between the parameters of the flowing fluid and the average pore radius (Figure 14c). Notably, the mainstream throat radius exhibited the strongest correlation (0.78) with movable fluid saturation. The results indicate that throat-related parameters exhibit stronger correlations with movable fluid characteristics than pore-related parameters, which suggests that the throat radius exerts a more prominent influence on the properties of movable fluids. Furthermore, a well-developed pore structure demonstrates a stronger correlation with movable fluids. The correlation between the parameters of the movable fluid and the mainstream throat radius shows a stronger relationship than the average throat radius. This difference can be attributed to the fact that the mainstream throat represents a specific subset of pores within the reservoir rock, and its size may provide a more accurate representation of the overall fluid flow behavior. On the other hand, the average throat radius considers all pores equally, which may not effectively capture the variations in pore size and connectivity within the reservoir. As a result, the mainstream throat's characteristics could exert a more significant influence on fluid saturation due to its specific role in governing fluid flow and distribution.

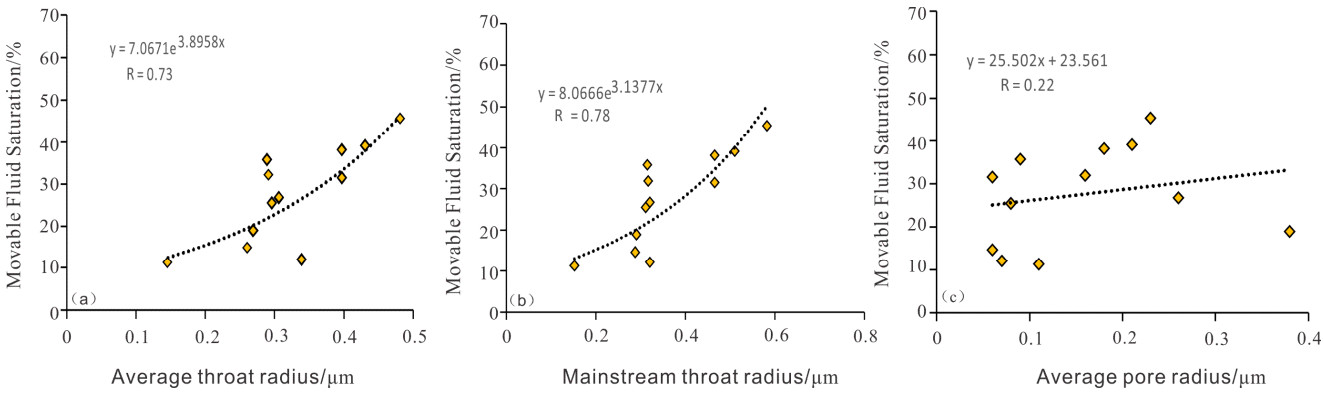

Figure 14. Corresponding relationship between reservoir pore structure and movable fluid saturation. (**a**) The relationship between average throat radius and movable fluid saturation; (**b**) The relationship between mainstream throat radius and movable fluid saturation; (**c**) The relationship between average pore radius with movable fluid saturation.

5.4. The Impact of Clay Minerals on Fluid Saturation

Numerous scientific investigations have been conducted to explore the mineralogical composition of tight rocks, along with their significant contributions and effects on the development of these formations as unconventional oil reservoirs [4]. According to the previous analysis, the average clay mineral content in the Chang 7 reservoir of the study area is 7.8%. The mineral composition primarily consists of illite (5.9%), followed by the chlorite group (3.7%) and kaolinite (3%) (Figure 3). Illite is distributed on the surfaces of clastic particles and within the pores as strands and bridges (Figure 6a). Kaolinite appears as the book leaves and develops as pore fillings within intergranular pores (Figure 6b). The chlorite group adopts a leaf-like shape and predominantly envelops the particle surfaces, serving as cushions within the pores (Figure 6c).

There is a distinct negative correlation between the content of clay minerals and movable fluid saturation (Figure 15). Clay minerals are distributed within the pore space, leading to a reduction in pore throat radius and the division of pores into numerous smaller ones. This phenomenon increases the resistance to fluid seepage, resulting in a further decrease in movable fluid saturation.

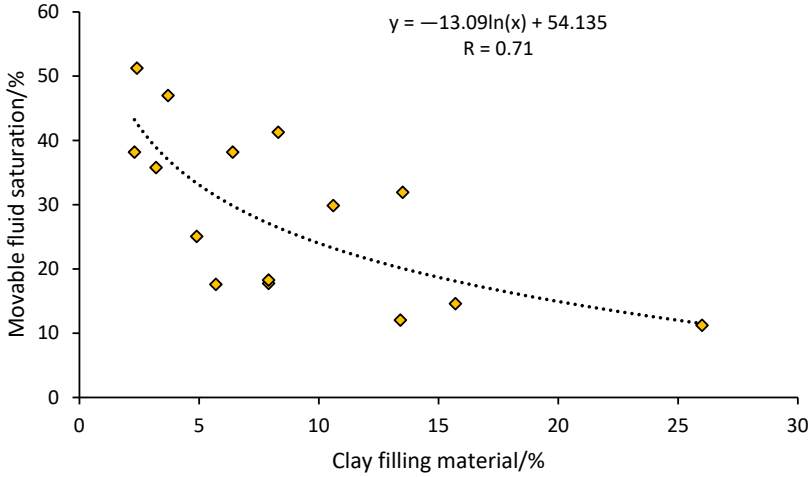

Figure 15. Corresponding relationship between clay−filling material and movable fluid saturation.

6. Conclusions

(1) The mainstream throat radius is a crucial indicator influencing core permeability in tight reservoirs. It directly reflects the seepage capability of the core, and smaller mainstream throat radii pose more significant challenges in extracting fluids from tight reservoirs.

(2) Studies indicate that in tight reservoirs, the permeability relationship with the saturation of movable fluids is more significant than its association with porosity. With increasing permeability, there is a corresponding increase in the movable fluid saturation. However, the movable fluid saturation relationship with porosity is weak.

(3) The parameters associated with throat radius in tight reservoirs significantly impact the behavior of movable fluids. The saturation of movable fluids exhibits stronger correlations with throat-related parameters than pore-related parameters. Notably, the correlation between movable fluid saturation and the mainstream throat radius surpasses that of the average throat radius. The size of the throat radius plays a paramount role in regulating fluid flow within the reservoir, as smaller throat radii impede fluid mobility. The content of clay minerals is also a crucial factor affecting the saturation of mobile fluids in the reservoir.

Author Contributions: Conceptualization, Q.W. and L.X.; software, H.Z.; validation, Q.W. and L.X.; formal analysis, H.Z.; investigation, H.Z.; resources, Y.H. and W.G.; writing—original draft preparation, Q.W.; writing—review and editing, Q.W. All authors have read and agreed to the published version of the manuscript.

Funding: This study was supported by the development demonstration project of large low-permeability lithologic stratigraphic reservoir in the Ordos Basin (2016zx00500). Characteristics of seismic rocks of the Yanchang formation in the Ordos Basin and geological significance (YCS22213069).

Data Availability Statement: Data not available due to commercial restriction.

Conflicts of Interest: The authors declare no conflict of interest.

References

1. Wei, Q.; Mei, J.; Tian, J.; Chen, X.; Xiao, L. Pore structure analysis of tight reservoirs in the He-8 Member of Upper Paleozoic in the southwestern Ordos Basin, China. *Interpretation* **2022**, *10*, 681–692. [CrossRef]
2. Xiao, L.; Bi, L.; Yi, T.; Lei, Y.; Wei, Q. Pore Structure Characteristics and Influencing Factors of Tight Reservoirs Controlled by Different Provenance Systems: A Case Study of the Chang 7 Members in Heshui and Xin'anbian of the Ordos Basin. *Energies* **2023**, *16*, 3410. [CrossRef]
3. Wu, L.; Zhang, J.; Jia, D.; Wang, S.; Yan, Y. Performance Evaluation of Multistage Fractured Horizontal Wells in Tight Gas Reservoirs at Block, M., Ordos Basin. *Energies* **2022**, *15*, 613. [CrossRef]

4. Saeed, S.A.; Hakimi, M.H.; Al-Muntaser, A.A.; Khamieva, A.N.; Varfolomeev, M.A.; Morozov, V.P.; Lashin, A.; Abdelaal, M.A.; Suwaid, M.A.; Mustapha, K.A.; et al. Geochemical, mineralogical and petrographical characteristics of the domanik formation from north samara region in the volga-ural basin, Russia: Implication for unconventional tight oil reservoir potential. *J. Pet. Sci. Eng.* **2023**, *220*, 111240. [CrossRef]
5. Durrani, M.Z.A.; Rahman, S.A.; Talib, M.; Subhani, G.; Sarosh, B. Characterization of seismic anisotropy using azimuthal AVO analysis (AVAz)—An application case study in the deep and tight carbonate reservoirs from Potwar Basin onshore Pakistan. *J. Appl. Geophys.* **2022**, *205*, 104767. [CrossRef]
6. Lai, J.; Wang, G.; Wang, Z.; Chen, J.; Pang, X.; Wang, S.; Zhou, Z.; He, Z.; Qin, Z.; Fan, X. A review on pore structure characterization in tight sandstones. *Earth-Sci. Rev.* **2018**, *177*, 436–457. [CrossRef]
7. Sakhaee-Pour, A.; Bryant, S.L. Effect of pore structure on the producibility of tight-gas sandstones. *AAPG Bull.* **2014**, *98*, 663–694. [CrossRef]
8. Temraz, M.G.; Mandur, M.M.; Coffey, B. Reservoir sedimentology and depositional environment studies of Alam El Bueib Formation using microfacies and nannofossils in Betty-1 well, Shoushan Basin, northern Western Desert, Egypt. *Environ. Geosci.* **2016**, *23*, 123–139. [CrossRef]
9. Xiao, L.; Yang, L.; Zhang, X.; Guan, X.; Wei, Q. Densification Mechanisms and Pore Evolution Analysis of a Tight Reservoir: A Case Study of Shan-1 Member of Upper Paleozoic Shanxi Formation in SW Ordos Basin, China. *Minerals* **2023**, *13*, 960. [CrossRef]
10. Daigle, H.; Johnson, A. Combining Mercury Intrusion and Nuclear Magnetic Resonance Measurements Using Percolation Theory. *Transp. Porous Media* **2015**, *111*, 669–679. [CrossRef]
11. Chandra, D.; Vishal, V. A critical review on pore to continuum scale imaging techniques for enhanced shale gas recovery. *Earth-Sci. Rev.* **2021**, *217*, 103638. [CrossRef]
12. Wang, C.; Zeng, J.; Lin, X.; Liu, X.; Wang, F.; Zhang, J.; Jia, K. Utility of GOI, QGF, and QGF-E for interpreting reservoir geohistory and oil remigration in the Hudson oilfield, Tarim basin, northwest China. *Mar. Pet. Geol.* **2017**, *86*, 486–498. [CrossRef]
13. Li, P.; Sun, W.; Wu, B.; Gao, Y.; Du, K. Occurrence characteristics and influential factors of movable fluids in pores with different structures of Chang 63 reservoir, Huaqing Oilfield, Ordos Basin, China. *Mar. Pet. Geol.* **2018**, *97*, 480–492. [CrossRef]
14. Mondal, I.; Singh, K.H. Fluid substitution in NMR T2 distribution and resistivity independent saturation computation using synthetic capillary pressure data. *Pet. Res.* **2023**, *8*, 77–78. [CrossRef]
15. Siavashi, J.; Najafi, A.; Sharifi, M.; Fahimpour, J.; Shabani, M.; Liu, B.; Liu, K.; Yan, J.; Ostadhassan, M. An insight into core flooding experiment via NMR imaging and numerical simulation. *Fuel* **2022**, *318*, 123589. [CrossRef]
16. Qu, Y.; Sun, W.; Tao, R.; Luo, B.; Chen, L.; Ren, D. Pore–throat structure and fractal characteristics of tight sandstones in Yanchang Formation, Ordos Basin. *Mar. Pet. Geol.* **2020**, *120*, 104573. [CrossRef]
17. Guo, Q.; Yao, Y.; Hou, L.; Tang, S.; Pan, S.; Yang, F. Oil migration, retention, and differential accumulation in "sandwiched" lacustrine shale oil systems from the Chang 7 member of the Upper Triassic Yanchang Formation, Ordos Basin, China. *Int. J. Coal Geol.* **2022**, *261*, 104077. [CrossRef]
18. Liu, X.; Li, S.; Guo, Q.; Zhou, X.; Liu, J. Characteristics of rock types and exploration significance of the shale strata in the Chang 73 sub-member of Yanchang Formation, Ordos Basin, China. *J. Nat. Gas Geosci.* **2021**, *6*, 363–373. [CrossRef]
19. Ji, L.-M.; Yan, K.; Meng, F.-W.; Zhao, M. The oleaginous Botryococcus from the Triassic Yanchang Formation in Ordos Basin, Northwestern China: Morphology and its paleoenvironmental significance. *J. Asian Earth Sci.* **2010**, *38*, 175–185. [CrossRef]
20. Zheng, R.; Zeng, W.; Li, Z.; Chen, X.; Man, K.; Zhang, Z.; Wang, G.; Shi, S. Differential enrichment mechanisms of organic matter in the Chang 7 Member mudstone and shale in Ordos Basin, China: Constraints from organic geochemistry and element geochemistry. *Palaeogeogr. Palaeoclim. Palaeoecol.* **2022**, *610*, 111126. [CrossRef]
21. Zhu, H.; Zhong, D.; Yao, J.; Sun, H.; Niu, X.; Liang, X.; You, Y.; Li, X. Alkaline diagenesis and its effects on reservoir porosity: A case study of Upper Triassic Chang 7 Member tight sandstone in Ordos Basin, NW China. *Pet. Explor. Dev.* **2015**, *42*, 56–65. [CrossRef]
22. Mahmud, W.M. Rate-Controlled Mercury Injection Experiments to Characterize Pore Space Geometry of Berea Sandstone. *E3S Web Conf.* **2023**, *366*, 01016. [CrossRef]
23. Wei, X.; Qun, L.; Shusheng, G.; Zhiming, H.; Hui, X. Pseudo threshold pressure gradient to flow for low permeability reservoirs. *Pet. Explor. Dev.* **2009**, *36*, 232–236. [CrossRef]
24. Li, P.; Jia, C.; Jin, Z.; Liu, Q.; Zheng, M.; Huang, Z. The characteristics of movable fluid in the Triassic lacustrine tight oil reservoir: A case study of the Chang 7 member of Xin'anbian Block, Ordos Basin, China. *Mar. Pet. Geol.* **2019**, *102*, 126–137. [CrossRef]
25. Singh, A.; Jha, N.K.; Mandal, P.P.; Esteban, L.; Desai, B.G. Pore throat characterization of bioturbated heterogeneous sandstone, Bhuj Formation, Kachchh India: An integrated analysis using NMR and HPMI studies. *J. Pet. Sci. Eng.* **2022**, *211*, 110221. [CrossRef]
26. Baban, A.; Al-Yaseri, A.; Keshavarz, A.; Amin, R.; Iglauer, S. CO_2–brine–sandstone wettability evaluation at reservoir conditions via Nuclear Magnetic Resonance measurements. *Int. J. Greenh. Gas Control.* **2021**, *111*, 103435. [CrossRef]
27. Li, T.; Huang, Z.; Zhao, J.; Xu, X.; Guo, X. Pore structure characteristics and their influencing factors: A case study from the middle jurassic mixed siliciclastic carbonate rocks, Turpan-Hami basin, Northwest China. *J. Pet. Sci. Eng.* **2021**, *203*, 108611. [CrossRef]

28. Mirzaei-Paiaman, A.; Ghanbarian, B. A new method for characterizing dynamic reservoir quality: Implications for quality maps in reservoir simulation and rock type classification. *J. Pet. Sci. Eng.* **2022**, *218*, 111049. [CrossRef]
29. Clarkson, C.; Freeman, M.; He, L.; Agamalian, M.; Melnichenko, Y.; Mastalerz, M.; Bustin, R.; Radliński, A.; Blach, T. Characterization of tight gas reservoir pore structure using USANS/SANS and gas adsorption analysis. *Fuel* **2012**, *95*, 371–385. [CrossRef]